ORIGINAL PAPER

Shallow unloading deformation analysis on Baihetan super-high arch dam foundation

Peng Lin[1] · Jie Shi[2] · Pengcheng Wei[1] · Qixiang Fan[3] · Zhilin Wang[3]

Abstract

The Baihetan super-high arch dam is the largest hydropower station in the world under construction. Columnar jointed basalt (CJB) is widely distributed at the Baihetan dam foundation, and the many closely spaced joints pose potential risks on the unloading quality of the foundation surface. In this study, typical unloading cracking and relaxation features of CJB based on field survey and the acoustic wave test are revealed during foundation excavation. Considering the large-scale joints in category-I CJB, an equivalent continuum constitutive model was proposed for describing anisotropic deformation and the unloading relaxation modes and the mechanism of columnar joints are further analysed. Both monitoring and numerical results show that: 1) the unloading behaviours include shallow relaxation of columnar joints and combined rebound deformation of columnar joints and shear belts; 2) the relaxation range of columnar joints mainly occurs at the shallow foundation surface with the maximum depth of 3~4 m, and the relaxation degree is obviously exaggerated owing to the sliding of shear belts; 3) the unloading relaxation mode at the shallow foundation mainly belongs to rebound deformation and relaxation of oral joints. The tensile failure occurs in steep joints, and both tensile and shear failure occur in gentle joints. The proposed model can be applied to effectively simulate the unloading relaxation processes of dam foundation excavation.

Keywords Equivalent continuum constitutive model · Shallow unloading deformation · Columnar jointed basalt · Relaxation mechanism · Baihetan super-high arch dam

Introduction

The dam interface is the contact surface between dam concrete blocks and foundation rockmasses, which transfers the huge water pressure from the dam body to the abutment rockmasses. Thus, the quality of foundation rockmasses and a matching dam interface are of great significance for the overall stability of a super arch dam (Lin et al. 2008, 2014, 2015, 2016, 2018; Zhang et al. 2013; Fan et al. 2015; Shen et al. 2017; Shi et al. 2018). Large-scale excavation is usually conducted for the foundation surface of super-high arch dams, which could cause unloading relaxation at shallow rockmass. The shallow unloading zone is generally defined as the rockmass zone below the excavation boundary where the physical, mechanical and hydraulic properties of the rockmasses have been significantly affected owing to blasting damage and stress redistribution (Wu et al. 2009; Malmgren et al. 2011; Chen et al. 2012).

The shallow unloading effects at foundation surface can certainly deteriorate the integrity and quality of dam foundation rockmass, easily causing sliding stability and seepage stability problems, particularly under high geo-stresses and complex geological conditions (Lin et al. 2008; Malmgren et al. 2011). For example, in Xiaowan super-high arch dam (with a height of 294.5 m), the maximum excavation depth in

✉ Peng Lin
celinpe@tsinghua.edu.cn

Jie Shi
sjthu13@163.com

Pengcheng Wei
wei-pc14@mails.tsinghua.edu.cn

Qixiang Fan
fan_qixiang@ctg.com.cn

Zhilin Wang
wang_zhilin@ctgpc.com.cn

[1] Department of Hydraulic Engineering, Tsinghua University, Beijing 100084, China

[2] Sichuan Airport Group Co., Ltd., Chengdu 610202, Sichuan, China

[3] China Three Gorges Corporation, Beijing 100038, China

the vertical and horizontal directions at the left abutment slope was 90 m and 130 m, respectively. The maximum geo-stress in the abutment slopes and at a depth of 40~50 m below the riverbed was 8~17 MPa and 22~35 MPa, respectively. Severe rockmass failure due to excavation unloading occurred at the shallow dam-foundation surface, including crack opening and sliding, onion skin relaxation, spalling and rock burst (Lin et al. 2008). As a result, the quality of local rockmasses at shallow foundation decreased significantly, and secondary excavation had to be conducted.

The unloading relaxation characteristic is generally influenced by many factors, such as the rockmass structure, geo-stress, geological conditions and irregular excavation outline. The Baihetan super-high arch dam is located in southwest China, which is the largest hydropower station in the world under construction. The geological conditions of the abutment slope of the Baihetan hydropower station are complicated owing to the existence of shear belts and a wide range of columnar jointed basalt (CJB). The columnar joint is a protogenetic tensile-cracking structure in basalt, which is usually formed owing to contraction of cooling solidified magma (Goehring et al. 2006). CJB has been found in many other dam sites, such as the Grand Coulee, Tongjiezi, Ertan and Xiluodu dams (Xu et al. 2011). However, the CJBs at the Baihetan arch dam site, which are very blocky with intensive joints and micro fissures, are widely distributed in the middle-low elevation of the dam foundation and underground caverns. Intensive unloading failure characteristics of CJB have been revealed in underground tunnels, such as loosening, falling and collapsing (Jin et al. 2015; Hao et al. 2016; Xiao et al. 2017). In terms of foundation excavation, Fan et al. (2017, 2018) comprehensively studied the unloading deformation and control measures of CJB and shear belts at dam foundation. However, the relaxation mode and mechanism of columnar joints is still not clear.

Besides field survey and test, a numerical method could also be used for studying the unloading relaxation mechanism of columnar joints. Both discrete and continuum models have been proposed for CJB. The discrete models can describe the discrete nature of jointed rockmass, and thus distinct element method (DEM) (Jin et al. 2018) and discontinuous deformation analysis (DDA) (Hatzor et al. 2015) have been applied for unloading failure modelling of CJB. However, the calculation range and efficiency of discrete model is limited for large scale of joints. For continuum models, the equivalent continuum method on the basis of deformation superposition is most widely used, which implicitly incorporates the mechanical features of discontinuities into the constitutive model (Wang and Huang 2009; Agharazi et al. 2012; Iwata et al. 2012). Those research works also provide effective methods for further investigating the unloading relaxation mode and mechanism of CJB.

This study aims to investigate the unloading relaxation mode and deformation mechanism of CJB during the excavation of the Baihetan dam foundation. On the basis of field survey, typical unloading failure features of CJB are firstly revealed. The unloading relaxation and disturbance degree of CJB are evaluated using acoustic wave tests. An equivalent continuum model considering joint spacing and connectivity was developed for CJB. On the basis of field monitoring and numerical simulation, the unloading relaxation modes and deformation mechanism of columnar joints are ultimately analysed.

Geological conditions at the Baihetan dam foundation

Topographical and geological conditions

The Baihetan hydropower station is located at Qiaojia and Ningnan county of southwest China. The hydropower station consists of an arch dam (height 289 m), spillway tunnels and two underground power generation system installed abutments, etc. It is the second largest hydropower station in the world and the largest hydropower station under construction with installed capacity of 16,000 MW.

The Baihetan arch dam is located at an asymmetrical V-shaped valley with gentle left slope and steep right slope, a width-to-depth ratio of about 1.75 (Fig. 1a). The river valley is 449~534 m wide at the normal reservoir water level. The rockmasses at the dam site are composed of Permian Emeishan basalt and breccia lava, including 11 layers of basalt $P_2\beta_1$-$P_2\beta_{11}$ with rock strata dipping towards the right bank (Fig. 1b, Fan et al. 2018). Faults and shear belts are widely developed at the dam site. The fault F_{17} is the largest fault in the left slope, outcropping at the foundation excavation surface. The faults F_{14} and F_{16} extend across the riverbed near the right abutment. The interlayer shear belts are mainly distributed on the top of each basalt layer. The interlayer shear belts C_3 and C_{3-1} in the left slope are revealed at elevation level (EL) 720~760 m. The interlayer shear belts C_3, C_{3-1}, C_4 and C_5 in the right slope are revealed at EL 640~780 m. The intrastratal shear belts Ls_{331}, Ls_{3318}, Ls_{3319}, Rs_{331} and Rs_{336} exist mainly in the third basalt stratum, i.e. $P_2\beta_3^{2-2}$ and $P_2\beta_3^3$. The occurrence and characteristics of main faults and shear belts are summarized in Table 1.

Structural properties of CJB

The CJB is mainly distributed in the layers $P_2\beta_3$–$P_2\beta_4$ at the dam foundation (Fig. 1b). According to the column length and diameter, the CJB can be divided into three categories (Shi et al. 2008). Category-I CJB has a slender size with the length of 2~3 m and diameter of 0.13~0.25 m (Fig. 2a). Category-II CJB has a moderate size with the length of 0.5~2 m and diameter of 0.25~0.5 m (Fig. 2b). Category-III CJB has a thick

Fig. 1 Topographical and geological conditions of the Baihetan arch dam: (a) topographical condition at the dam site; (b) geological profile along the dam axis (Fan et al. 2018)

(a)

(b)
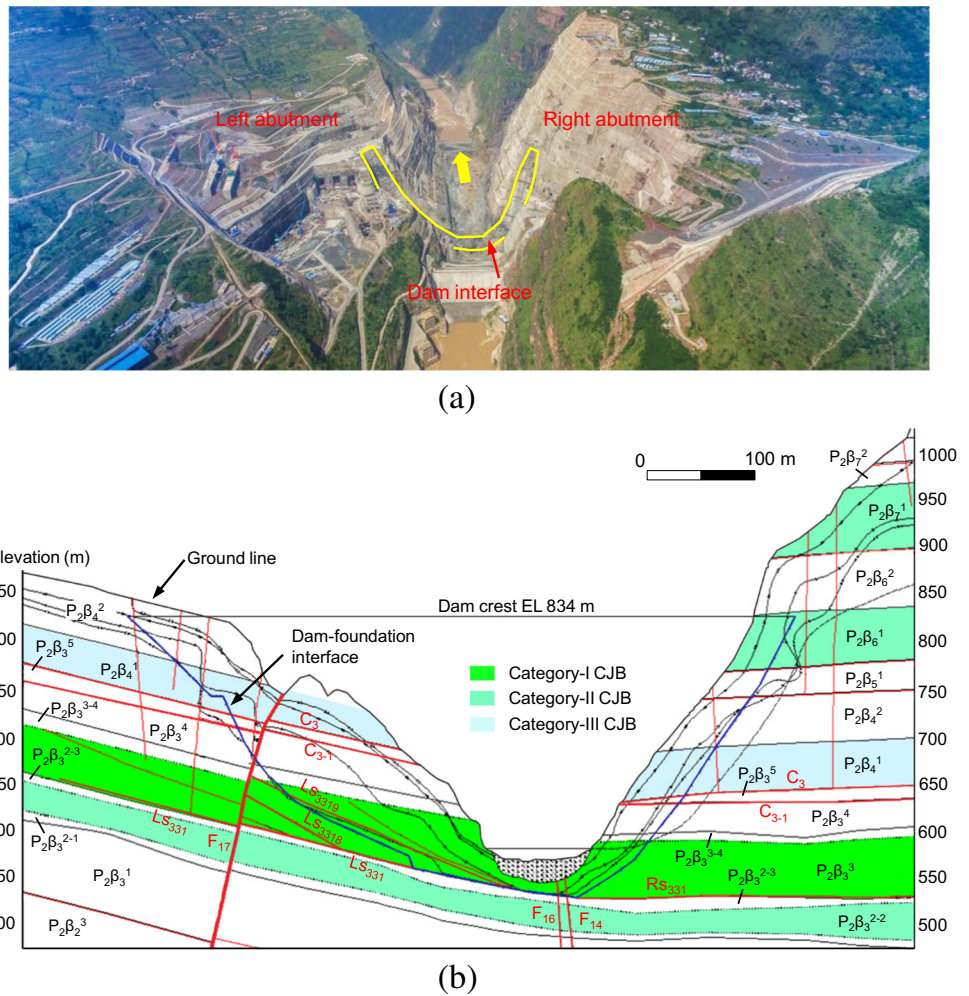
size with the length of 1.5~5 m and diameter of 0.5~2.5 m (Fig. 2c). The geometrical and mechanical parameters of CJB are listed in Table 2 (Shi et al. 2015).

Table 1 Summary of the occurrence of main structural planes

Set	Average occurrence	Remarks
1	N35°E∠75° NW	The largest fault F_{17} cuts across the left abutment foundation, stretching for 1 km. The fault width varies between 1.2 and 2.4 m, containing breccia and cataclasite rocks.
2	N60°W∠80–90°NE	The second largest fault F_{14} stretches for 850 m, with width varying between 0.5 and 1.4 m. Fault F_{16} cuts across the right abutment foundation, containing breccia and cataclasite rocks.
3	N30°E∠10–35°SE	The set includes most of the shear belts, such as C_3, C_{3-1}, C_4, C_5, Ls_{331}, Ls_{3318}, Ls_{3319}, Rs_{331} and Rs_{336}. The interlayer shear belts contain tuff. The intrastratal shear belts contain tectonite, with width varying between 0.05 and 0.3 m.

Among the three categories, most closely spaced joints are developed in category-I CJB. Except for the columnar joint, many micro fissures are distributed in the column (Fig. 3a), such as micro fissures parallel to the columnar joint (steep fissure) and perpendicular to the columnar joint (gentle fissure). The typical columns do not have the ideal hexagonal cross sections. The proportion of quadrangular, pentagonal and hexagonal polygons in the columns is 32.1%, 46.7% and 17.6%, respectively (Jiang et al. 2014). The length of columnar joint is usually less than 2 m, with average dip angle of 70°. The dip angle of the steep fissure is slightly steeper than that of the columnar joint and the trace length of the steep fissure is about 0.3~2 m. The gentle fissure is short with the trace length of 0.003~0.2 m, which cuts the column incompletely. The dip angle of gentle fissure is about 10~30°, which is nearly parallel to the rock layer. In addition, many random and micro fissures cut the column into small blocks (Fig. 3b).

The category-I CJB is mainly distributed at EL 665~570 m in the left slope and EL 590~545 m in the right slope. Figure 4 shows the integrity of rock cores obtained from field drilling, which is conducted at the
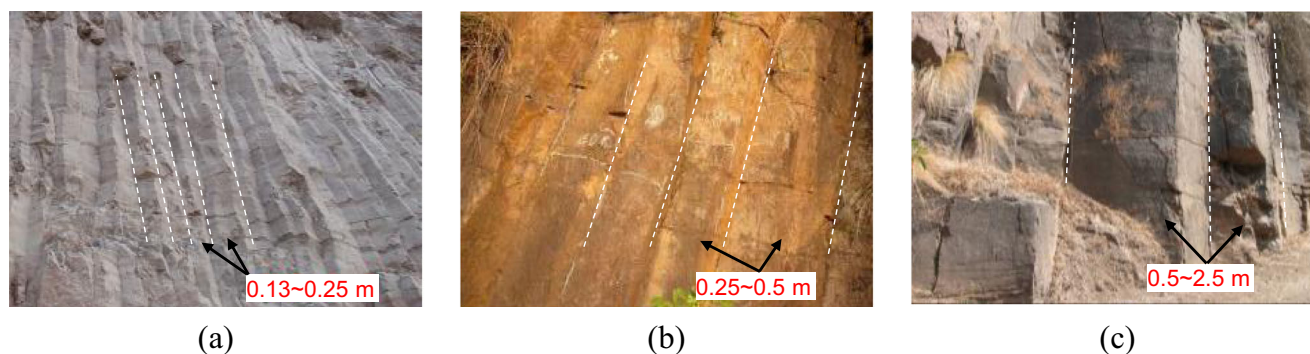
Fig. 2 Classification of CJB: (a) category-I CJB; (b) category-II CJB; (c) category-III CJB

typical location of category-I CJB revealed at the left foundation. It can be seen that the quality and integrity of category-I CJB at shallow foundation is poor. The developed joints and fissures cause loose rock after unloading, and the minimum size of rock is about 0.05 m. With the increase of drilling depth, the integrity of category-I CJB gradually improves. Thus, owing to the large-scale joints, the unloading cracking and relaxation of category-I CJB under excavation could present a great challenge for the rockmass quality of the dam interface.

Geo-stress

Geo-stress is also an important factor that affects the unloading relaxation degree. At the Baihetan dam site, the geo-stresses are mainly measured by the stress relief and hydro fracturing methods at the dam site (Shi et al. 2015). The results show that the horizontal stress is higher than the gravitational stress owing to the existence of tectonic stress. At the left bank, the maximum, intermediate and minimum principal stresses are 5.0~7.5 MPa, 4.1~4.9 MPa and 3.7~5.1 MPa, respectively. At the right bank, the maximum, intermediate and minimum principal stresses are 5.1~9.4 MPa, 4.7~7.5 MPa and 3.8~6.4 MPa, respectively. At the river bed, the maximum horizontal principal stresses at the foundation depth of 40 m, 70 m and 130 m are 3~6 MPa, 6~12 MPa and 22~28 MPa, respectively. In terms of foundation surface, the maximum geo-stress measured at hanging wall of Ls_{3319} and Ls_{331} of left bank is 3~4 MPa and 6~7 MPa, respectively.

Unloading cracking and relaxation features of CJB

Unloading cracking features

The unloading cracking features of columnar jointed basalt were revealed during excavation of the dam foundation, such as shallow relaxation of columnar joints, combined rebound deformation of columnar joints and shear belts.

Shallow relaxation of columnar joints

The surface layer of columnar joints became loose along the dam interface after excavation unloading (Fig. 5a). According to the drilling TV, three types of relaxation of columnar joints were revealed with time-spatial revolution at shallow foundation. Each picture in Fig. 5b, c and d refers to unloading relaxation development of columnar joints at different times since the excavation was done from Nov. 2014 to Jan. 2015. Owing to blast effect and excavation unloading, the superficial CJB were severely damaged with loose rock. With the development of unloading, local rocks collapse from the drilling wall, decomposing the column into small blocks (Fig. 5b). Many steep joints and fissures were observed in drilling TV. Under the excavation unloading, the steep joints in shallow foundation gradually opened with tensile cracking (Fig. 5c). Additionally, the gentle joints in deep foundation gradually opened under the stress adjustment (Fig. 5d). It can be seen that the unloading relaxation and stress adjustment are not finished immediately. Under the foundation excavation,

Category	Column size		Deformation modulus (GPa)		Shear strength	
	Length (m)	Diameter (cm)	Horizontal direction	Vertical direction	Cohesion c (MPa)	Friction coefficient f
Category-I	2~3	13~25	9~11	7~9	1.0~1.2	1.0~1.2
Category-II	0.8~1.2	25~50	14~18	10~12	1.3~1.5	1.2~1.4
Category-III	3~5	>50	17~20	17~20	1.4~1.7	1.3~1.4

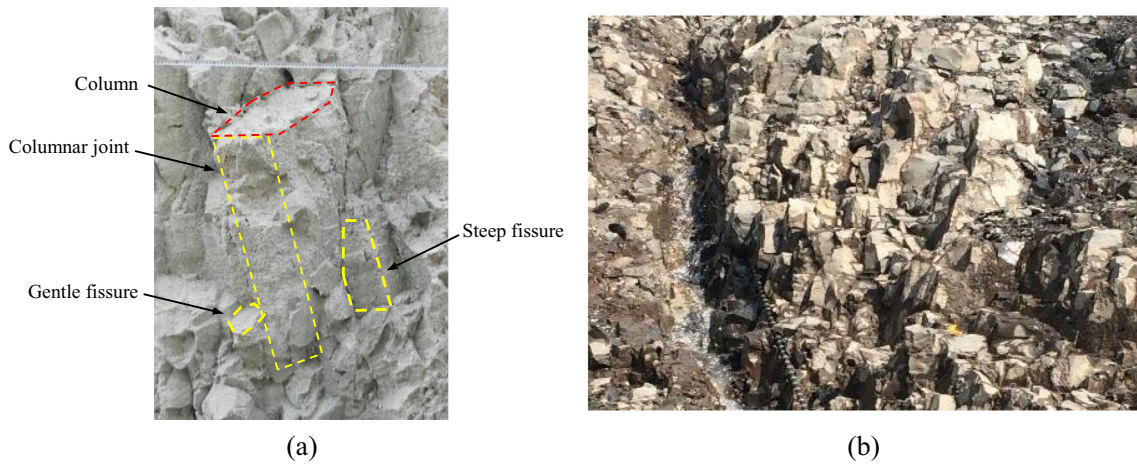Table 2 Geometrical and mechanical parameters of columnar jointed basalt (Shi et al. 2015)

Fig. 3 Structural features of category-I CJB at dam foundation: (a) three types of joints; (b) site view of category-I CJB

the unloading relaxation tends to be stable in 1–2 months, which belongs to normal stress adjustment.

Combined rebound deformation of columnar joints and shear belts

The left abutment is cut by several shear belts, which forms a typical combined block consisting of persistent shear belt and mosaic columns. Under the large scale excavation, shear deformation occurred in the intrastratal shear belt Ls_{3319}. Cracking of shear belt Ls_{3319} was found in the drainage and grouting tunnels close to the foundation surface (Fig. 6a, b).

The sliding of Ls_{3319} also caused cracks of the shotcrete layer (Fig. 6c). In addition, the relaxation of columnar joints were obviously exaggerated by the sliding of shear belt Ls_{3319}. At the edge of Ls_{3319} below EL 665 m, large scale joint cracking and opening were observed (Fig. 6d).

Unloading relaxation depth

To evaluate the rockmass quality and relaxation depth, the acoustic wave test was used after foundation excavation. Figure 7a shows the layout of acoustic wave tests at the left foundation, in which EL 660~650 m is chosen as the
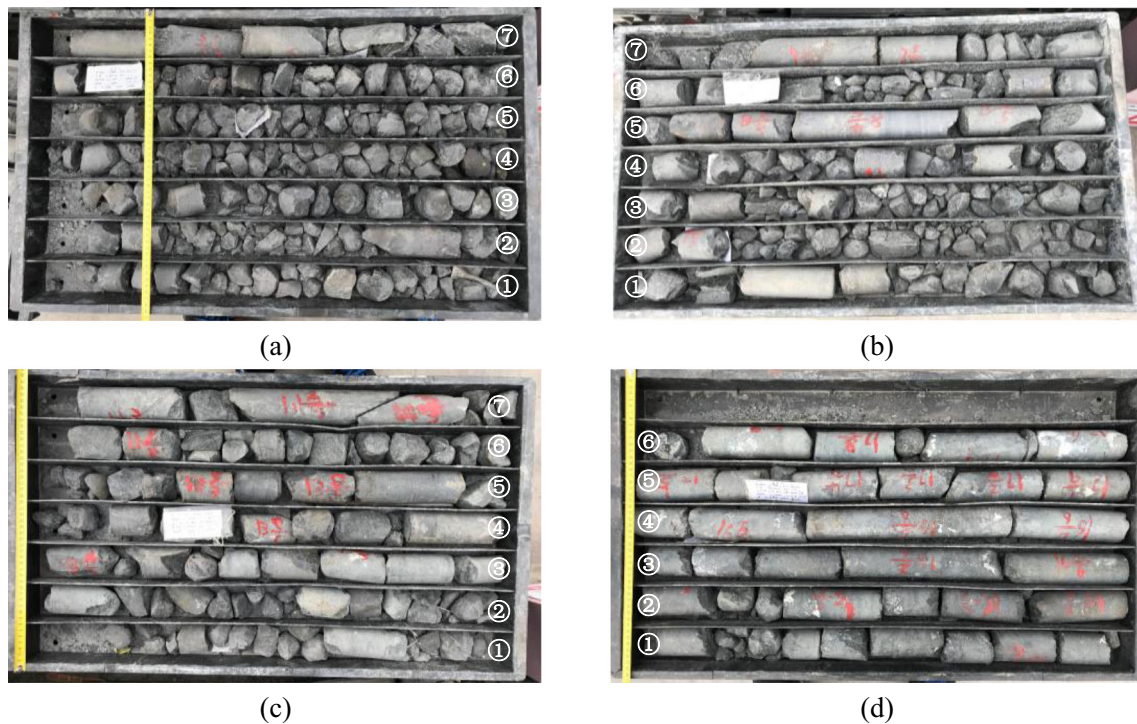

Fig. 4 Integrity variation of category-I CJB with drilling depth at dam foundation: (a) 0~6.5 m; (b) 6.5~12 m; (c) 15~20 m; (d) 20~25 m
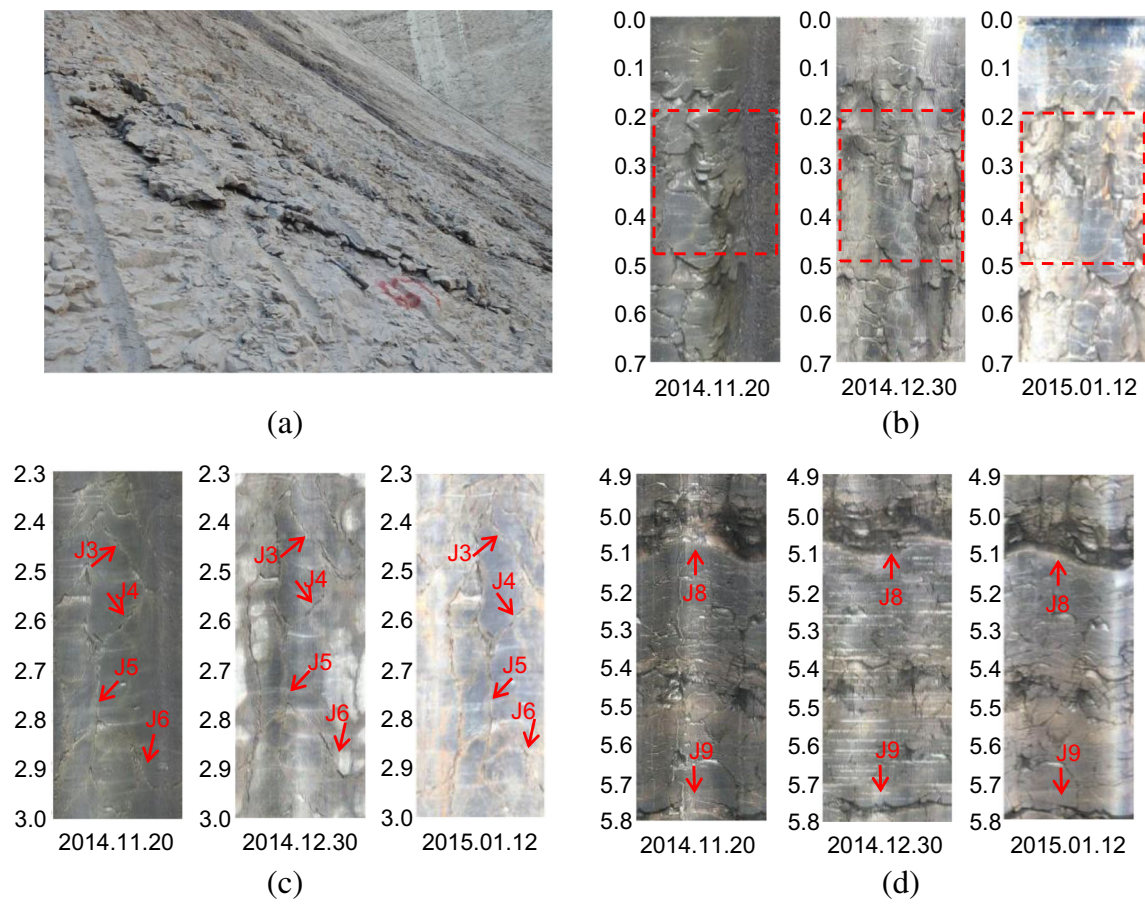
Fig. 5 Shallow relaxation of columnar joints: (a) superficial relaxation of joints along the foundation surface; (b) rock damage and collapse at surface layer; (c) steep joints open at shallow foundation; (d) gentle joints open at deep foundation
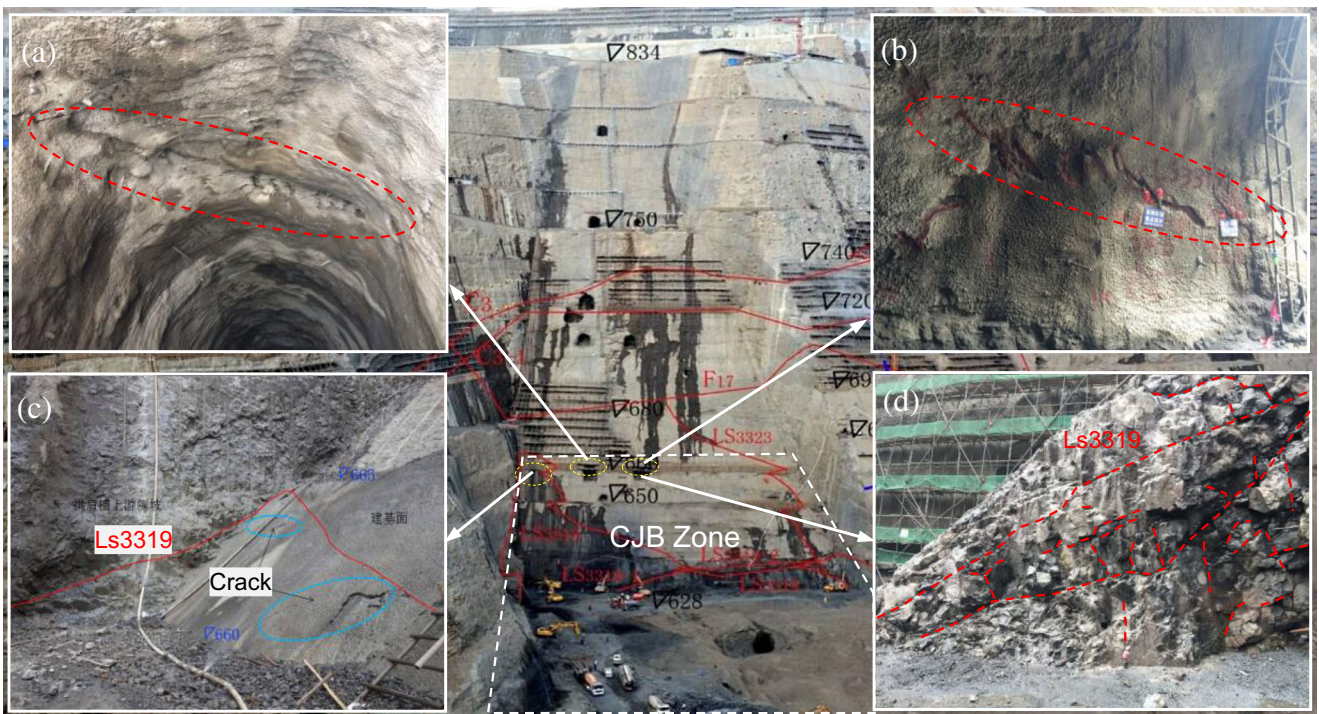

Fig. 6 Combined rebound deformation of columnar joints and shear belts: (a) cracking in grouting tunnel WML-2; (b) cracking in drainage tunnel PSL-2; (c) cracking of shotcrete; (d) combined relaxation of columnar joints and shear belts
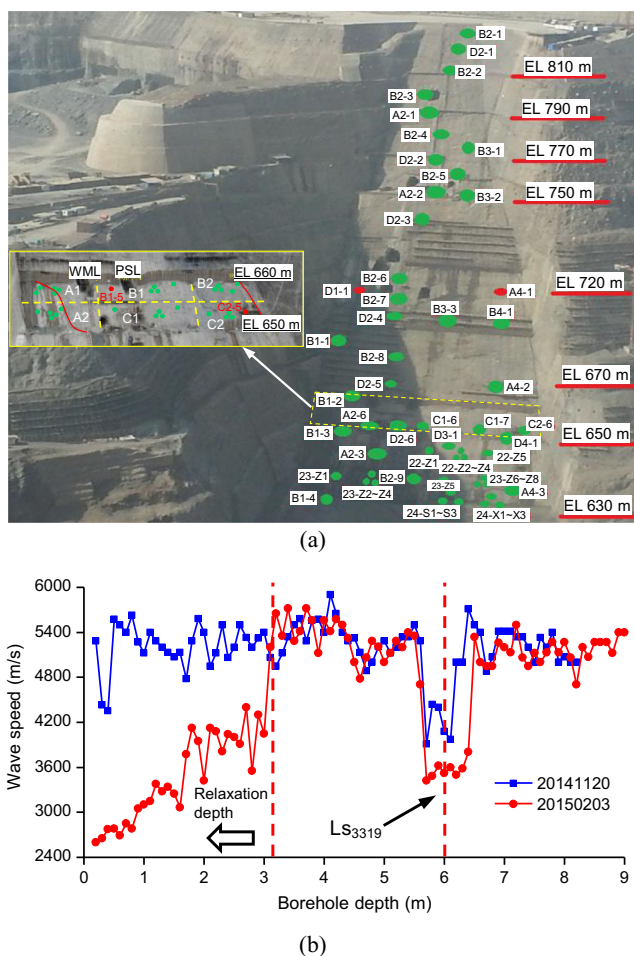
(a)

(b)

Fig. 7 Monitoring layout of acoustic boreholes at left foundation: (a) layout of acoustic boreholes; (b) relaxation depth division based on wave speed

experimental zone of category-I CJB. The longitudinal wave was measured in the borehole perpendicular to the foundation surface. On the basis of the longitudinal wave speed in undisturbed condition (Table 3), the relaxation depth of foundation rockmass after excavation could be defined according to the decreasing range of wave speed (Fig. 7b).

Compared with wave speed after unloading, the relaxation depth of CJB was larger than other rockmasses (Fig. 8). For

Table 3 Wave speed of foundation rock mass under undisturbed condition (Shi et al. 2015)

Rock mass classification	Property of rock	Wave speed (m/s)
II	Non-CJB	>4700
III$_1$	Non-CJB	4200~4700
	CJB	4700~5100
III$_2$	Non-CJB	3500~4200
	CJB	4000~4700

example, the borehole B4–1 (EL 695 m) was located at the non-columnar joints zone with relaxation depth of 0.8 m (Fig. 8a). The borehole A4–3 (EL 634 m) was located at the columnar joints zone with relaxation depth of 2.8 m (Fig. 8b). The boreholes B1–5 (EL 658 m) and C2–5 (EL 654 m) at experiment zone had relaxation depth of 3.3 m and 4.4 m, respectively. In addition, the relaxation depth developed over time, which tended to be stable in 1~2 months.

The stable relaxation depth was finally counted at left abutment (Fig. 9a). Owing to the combined relaxation of category-I CJB and shear belt Ls$_{3319}$, the relaxation depth at the experimental zone was larger than other locations. The average relaxation depth at the left foundation above EL 665 m was 1.71 m. The average relaxation depth of category-I CJB below EL 665 m was 2.18 m. In particular, at the field test zone, the average relaxation depth in area A was 1~2 m, while the average relaxation depth in areas B and C was 3~4 m (Fig. 9b).

Under excavation unloading, the average relaxation depth of category-I CJB is larger than other rockmasses. In addition, the weak shear belt has unfavourable influence on the relaxation degree of CJB. For example, at the field test zone, the rockmass quality in area A is better than that in areas B and C (Fig. 10), and unloading relaxation in areas B and C were further exaggerated owing to sliding of shear belts. Particularly, the combined rebound deformation of columnar joints and shear belts results in the largest relaxation depth at the dam foundation.

Unloading disturbance degree

In the relaxation zone, the disturbance degree is different owing to different degrees of unloading and blast damage. Gardner et al. (1974) found that the density of relaxed rockmass could change with longitudinal wave speed and established the following equation.

$$\rho_p = 0.31 V_p^{0.25} \tag{1}$$

where ρ_p is the density of relaxed rockmass, and V_p is the longitudinal wave speed of relaxed rockmass.

Shen et al. (2016) further established the unloading disturbance factor D based on longitudinal wave speed and density, which could well reflect the unloading disturbance degree.

$$D = 1 - \frac{\rho_p V_p^2}{\rho_0 V_0^2} \tag{2}$$

where ρ_0 is the density of non-relaxed rockmass. V_0 is the longitudinal wave speed of non-relaxed rockmass.

After excavation, the dam foundation was divided into different layers based on the wave speed, such as 0~1 m, 1~3 m, 3~6 m, 6~10 m, 10~15 m and 15~20 m below the foundation surface. Considering the category-I CJB at EL 660~628 m, the

Fig. 8 Variation of longitudinal wave speed of rock masses under excavation unloading: (a) B4–1 (EL 695 m); (b) A4–3 (EL 634 m); (c) B1–5 (EL 658 m in the experimental zone); (b) C2–5 (EL 654 m in the experimental zone)
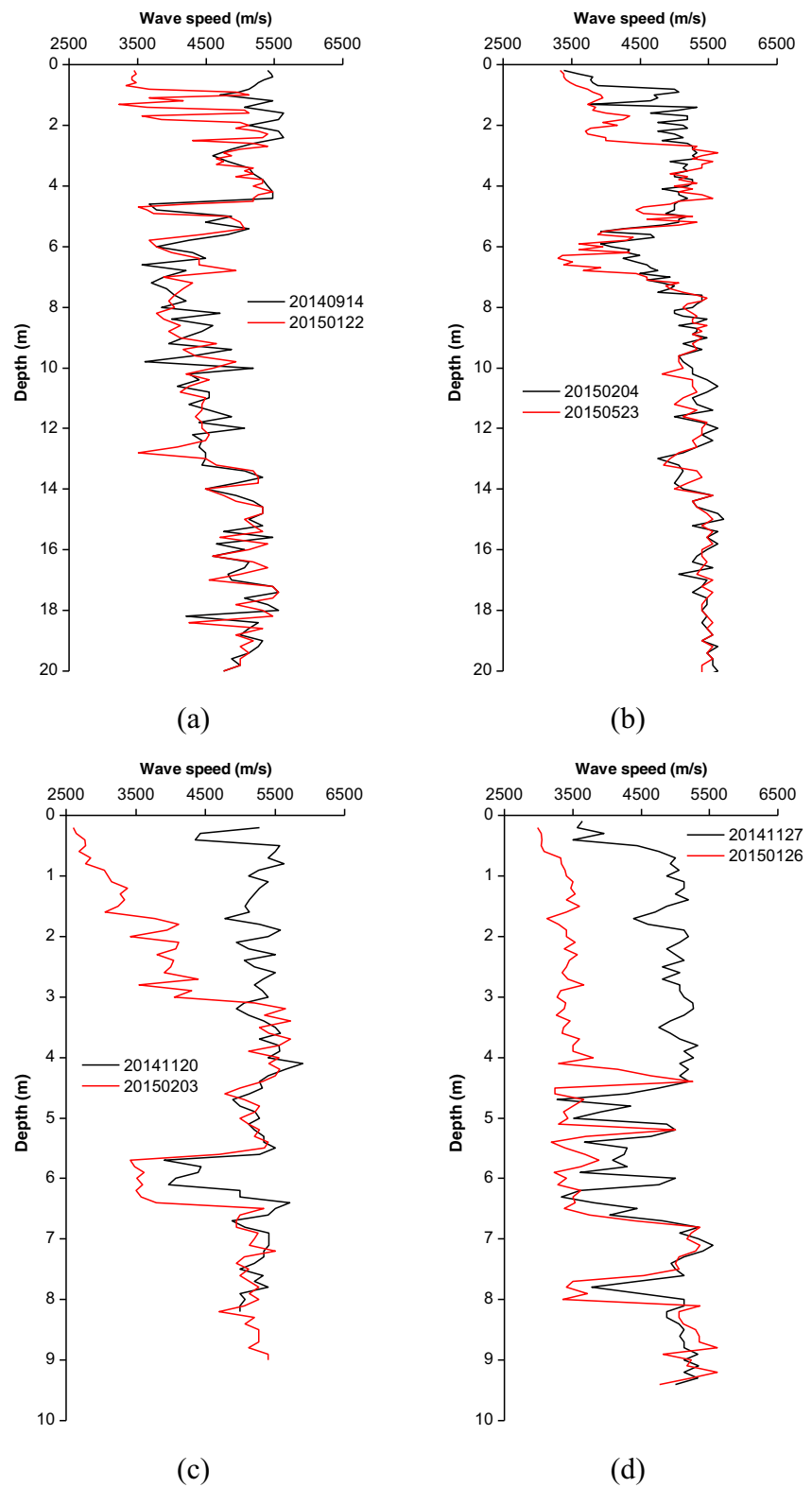
average wave speed after excavation at 0~1 m, 1~3 m, 3~6 m, 6~10 m, 10~15 m and 15~20 m depth of foundation was 4035 m/s, 4631 m/s, 5025 m/s, 5206 m/s, 5359 m/s and 5446 m/s, respectively.

It can be seen that the wave speed at depth of 6~20 m is stable, which could be regarded as an undisturbed state with average speed of 5300 m/s. Equation (2) is then used to evaluate the unloading disturbance degree of category-I CJB. As
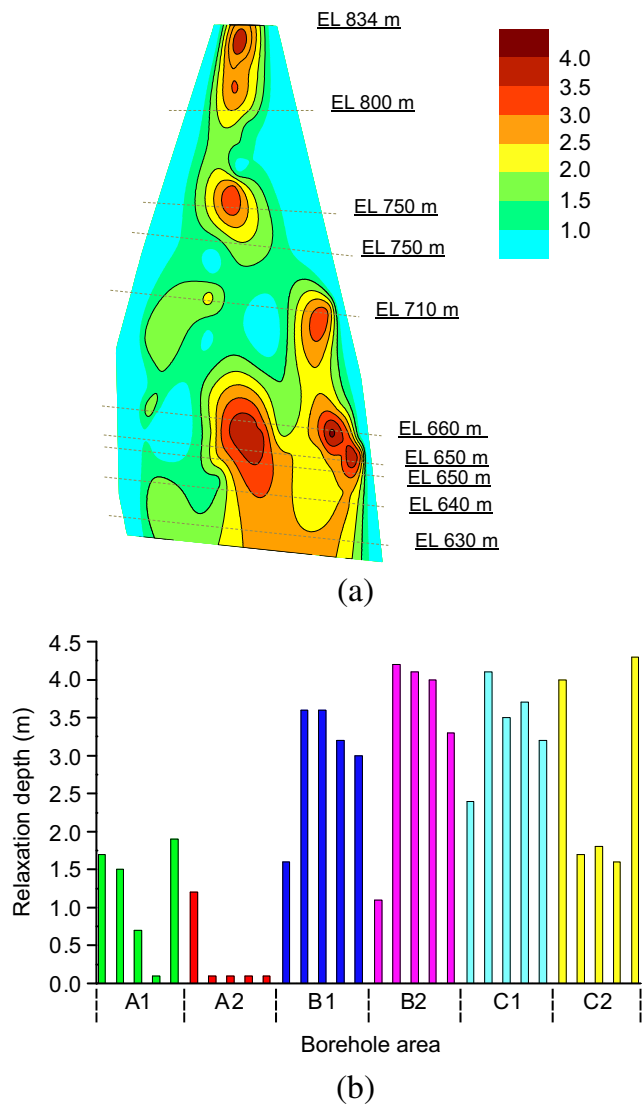
Fig. 9 Unloading relaxation depth: (a) at the left foundation (unit: m); (b) at the experimental zone

shown in Fig. 11, the disturbance mainly occurs at the shallow foundation of 2~6 m depth, and the disturbance factor D is 0.05~0.27. The disturbance at the superficial rock layer of 1 m depth is relatively large with disturbance factor D of 0.48, which is consistent with the field relaxation features.

Numerical analysis of shallow unloading deformation characteristics

Equivalent continuum constitutive model

Deformation constitutive model of jointed rockmass

Considering the large-scale joints in category-I CJB, the equivalent continuum constitutive model was proposed for describing anisotropic deformation and failure behaviours, which can implicitly incorporate the discontinuities into constitutive equations. On the basis of the principle of strain superposition, the total strain increment of jointed rockmass could be calculated as the sum of equivalent rockmass and multiple joint sets.

$$d\varepsilon = d\varepsilon^{I} + d\varepsilon^{J} \tag{3}$$

where $d\varepsilon^{I}$ is the strain increment of equivalent rockmass, and $d\varepsilon^{J}$ is the strain increment of all joint sets.

On the basis of the deformation constitutive model developed by Agharazi et al. (2012), the strain increment of all joint sets can be expressed as:

$$d\varepsilon^{J} = \sum_{a=1}^{M} d\varepsilon^a = \sum_{a=1}^{M} \frac{1}{S^a} \mathbf{T}^{a^T} \mathbf{D}^a \mathbf{T}^a d\sigma \tag{4}$$

where M is the joint set number, S^a is the spacing of joint set a, $\mathbf{T}^a$ is the transformation matrix between local axis and global axis and $\mathbf{D}^a$ is the compliance matrix of joint plane a and can be written as:

$$\mathbf{D}^a = \begin{bmatrix} D_{nn} & D_{ns} & D_{nt} \\ D_{sn} & D_{ss} & D_{st} \\ D_{tn} & D_{ts} & D_{tt} \end{bmatrix} \tag{5}$$

For simplicity, only the normal compliance D_{nn} and the shear compliance D_{ss}, D_{tt} ($D_{tt} = D_{ss}$) were considered.

Thus, the compliance matrix of all joint sets can be expressed as:

$$\mathbf{C}^{J} = \sum_{a=1}^{M} \frac{1}{S^a} \mathbf{T}^{a^T} \mathbf{D}^a \mathbf{T}^a \tag{6}$$

After the compliance matrix $\mathbf{C}^{I}$ and $\mathbf{C}^{J}$ are obtained, the equivalent compliance matrix of jointed rockmass $\mathbf{C}^{eq}$ can be expressed as:

$$\mathbf{C}^{eq} = \mathbf{C}^{I} + \mathbf{C}^{J} \tag{7}$$

Thus, the total strain increment of jointed rockmass can be written as:

$$d\varepsilon = d\varepsilon^{I} + d\varepsilon^{J} = \mathbf{C}^{I} d\sigma + \mathbf{C}^{J} d\sigma = \mathbf{C}^{eq} d\sigma \tag{8}$$

Failure criterion of rock and joints

A composite Mohr-Coulomb criterion with tension cut-off is used for equivalent rockmass and joints. The shear and tensile failure criterion of equivalent rockmass can be expressed as:
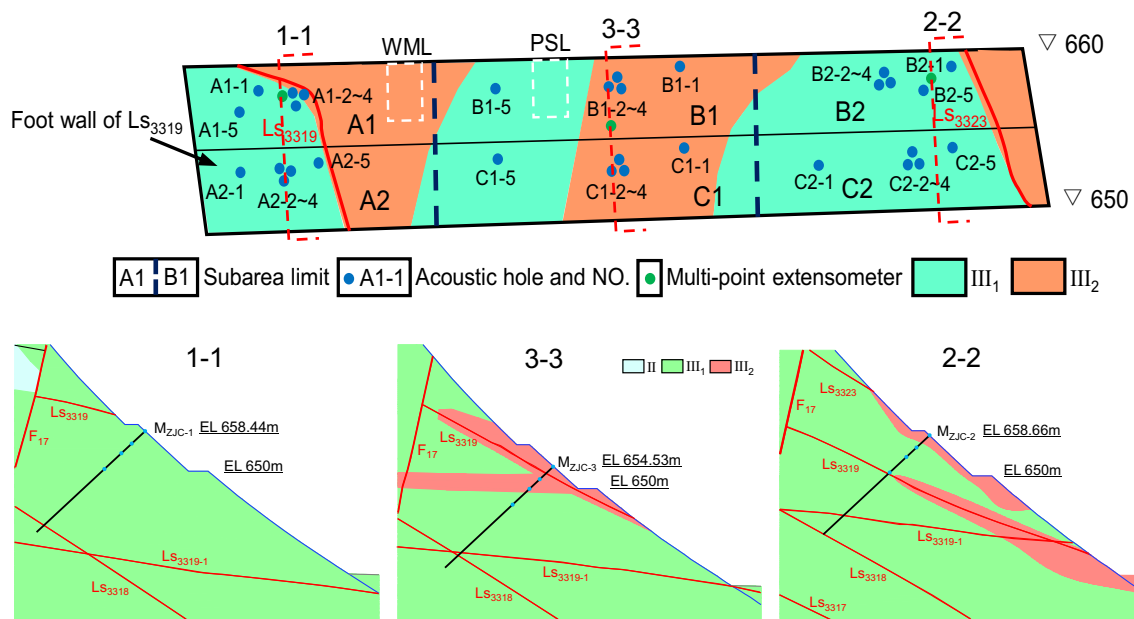
Fig. 10 Subarea division and rock mass quality at the field test zone

$$F_{si} = c_i + \sigma_{ni}\tan\phi_i \qquad (9)$$

$$F_{ti} = \sigma_{1i} - \sigma_{ti} \qquad (10)$$

where c_i is the cohesion of rock, σ_{ni} is the normal stress on the rock, ϕ_i is the friction angle of rock, σ_{1i} is the maximum principal stress of rock and σ_{ti} is the tensile strength of rock.

For the joint set, the shear and tensile failure criterion can be expressed as:

$$F_{sj} = c_j + \sigma_{nj}\tan\phi_j \qquad (11)$$

$$F_{tj} = \sigma_{1j} - \sigma_{tj} \qquad (12)$$

Fig. 11 Variation of unloading disturbance factor with borehole depth

where c_j is the cohesion of joint, σ_{nj} is the normal stress on the joint, ϕ_j is the friction angle of joint, σ_{1j} is the maximum principal stress of joint and σ_{tj} is the tensile strength of joint.

Modification of deformation and shear strength of non-persistent joint

For the staggered joint set, Singh (1973) proposed the stress concentration factor under different stress state considering the staggered distance for orthogonal joint sets (Fig. 12).

$$B_{N1} = \left[1 + \frac{K_{T2}S}{K_{N1}S_2}\left(1 - \frac{S}{S_1}\right)\right]^{-1} \qquad (13)$$

$$B_{T1} = \left[1 + \frac{K_{N2}S}{K_{T1}S_2}\left(1 - \frac{S}{S_1}\right)\right]^{-1} \qquad (14)$$

where B_{N1} and B_{T1} are the normal and shear concentration factors, respectively. K_N and K_T is the normal and shear stiffness, respectively.

On the basis of Jennings' criterion (1970), the shear strength of a non-persistent joint is simply determined as the linear weighted average of the strength of the joint and the rock bridge. Thus, the equivalent shear strength of transverse joint could be revised as:

$$f_{eq} = kf_i + (1-k)f_j = f_j + k\left(f_i - f_j\right) \qquad (15)$$

$$c_{eq} = kc_i + (1-k)c_j = c_j + k\left(c_i - c_j\right) \qquad (16)$$

where f_{eq} and c_{eq} are the equivalent friction coefficient and the cohesion of non-persistent joint plane, respectively. k is the
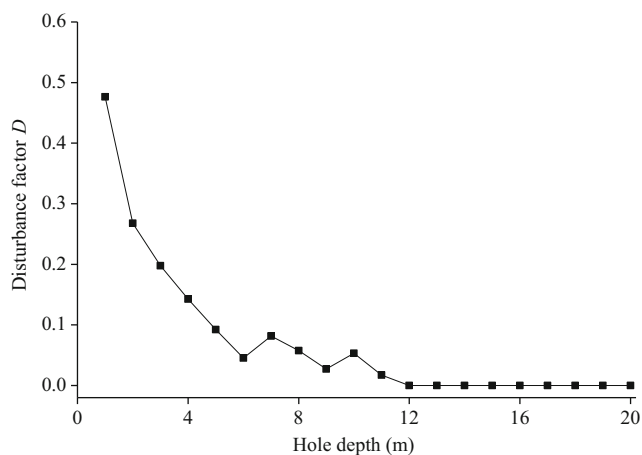
joint persistence, which is defined as the area of the intact rock to the total area of joint plane.

Simulating method and analysis cases

Excavation modelling

The left abutment slope is selected for analysis on unloading deformation and cracking of foundation rockmasses (Fig. 13a). The excavation process from EL 834 m to EL 540 m in the left slope is analysed. The typical section along the dam axis is chosen for analysis, where most structural planes and category-I CJB are encountered (Fig. 13b). The faults and shear belts, including the fault F_{17}, the interlayer shear belts C_3 and C_{3-1}, and the intrastratal shear belts L_{S3319}, $L_{S3319-1}$, L_{S3318} and L_{S331} are considered in the numerical model.

The equivalent continuum constitutive model was used for category-I CJB, while other rockmasses adopted the elastic-plastic model with Mohr-Coulomb criterion. When modelling shear belts, Ls_{3319} and Ls_{3319-1} adopted non-thickness contact element with the Coulomb shear model. Other shear belts and faults adopt the thin-layer solid element with Mohr-Coulomb criterion. In terms of boundary condition, the left boundary was fixed in the normal direction and right boundary was modelled with horizontal tectonic stress, which can obtain the initial stress field before excavation.

Material parameters

The equivalent continuum model is adopted to analyse the unloading deformation and cracking behaviours of category-I CJB at the dam foundation. The columnar joints with a dip angle of 70 degree and gentle joints with a dip angle of 20 degree are considered as two primary joint sets (Fig. 13b). In
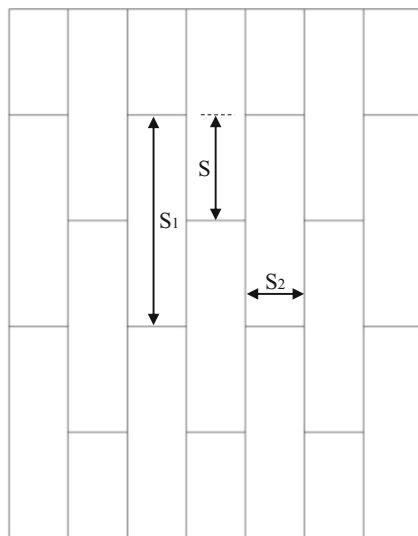

Fig. 12 Schematic of staggered joint sets

addition, the non-persistent gentle joint set has a connectivity ratio of 0.5, which cut the columns with the length of 2~3 m. The physical and mechanical parameters of rockmasses adopted in the numerical model are summarized in Table 4 (Shi et al. 2015). The deformation and shear strength parameters of rockmasses, fault and shear belts are obtained with rigid bearing plate and direct shear test at field, respectively (Shi et al. 2015). Table 5 lists the deformation and strength parameters of category-I CJB, which include the equivalent mechanical parameters that take into consideration the aphanitic microcracks and the joint surface parameters of the discretized original joints (Jin et al. 2015). The equivalent mechanical parameters were obtained on the basis of laboratory compression tests, direct shear tests and Brazilian disk experiments. The deformation parameters of the joint surface were determined with Young's modulus of equivalent rockmass, intact rockmass and joint space (Jin et al. 2015). The internal friction angle of the original joint surface was obtained by laboratory shear test.

Geo-stress inversion and analysis cases

Inversion of initial geo-stress field was firstly conducted at the typical section of left foundation. To obtain the initial stress field before excavation, right boundary was modelled with horizontal tectonic stress. On the basis of the field geo-stress result at the depth of foundation surface, the maximum geo-stress obtained at hanging wall of Ls_{3319} and Ls_{331} in numerical model is about 3~4 MPa and 6~7 MPa, respectively.

At EL 660~650 and below EL 650, 2 m and 5 m protective layers are reserved (Fig. 13a). The process of foundation excavation can be simplified in the following steps: (1) The foundation is excavated from EL 834 m to EL 628 m, except for the persevered protective layers. During the excavation from EL 645 m to EL 628 m, an inverse analysis of rockmass parameters is then conducted for category-I CJB and shear belt based on measured displacement and relaxation depth. (2) The foundation is excavated from EL 628 m to EL 620 m except for protective layers. (3) The protective layer is excavated from EL 660 m to EL 620 m. (4) Prestressed anchorage cables with pretension of 3000 kN and spacing of 2 × 2 m are installed at dam-foundation surface. (5) The foundation is excavated from EL 620 m to EL 545 m except for protective layers. (6) The protective layer is excavated from EL 620 m to EL 540 m.
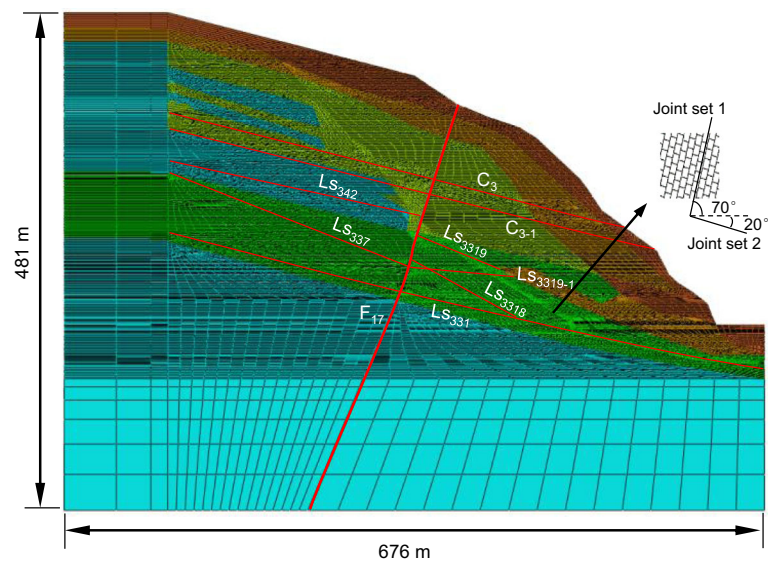
Unloading deformation analysis

The multi-point extensometer and joint meter are used to monitor the deformation of category-I CJB and shear belts (Fig. 14), respectively. Multi-point extensometers were installed at the experimental zone, which were perpendicular to the foundation surface with the maximum depth of

Fig. 13 Excavation scheme and mesh model of the Baihetan left slope: (a) excavation scheme; (b) mesh model
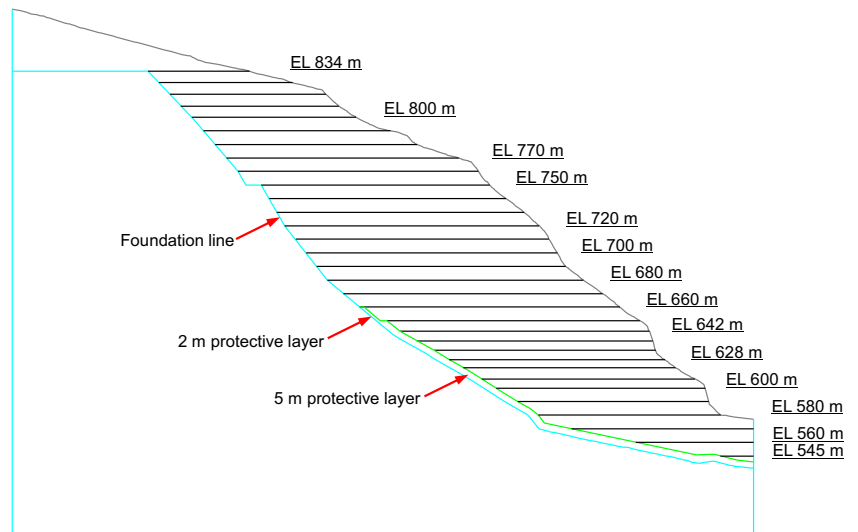
(a)

(b)

32 m. Joint meters were installed to monitor the shear deformation of shear belts.

The unloading deformation of category-I CJB is firstly compared between numerical and measured results during the excavation from EL 645 m to EL 628 m. The multi-point extensometers M_{ZJC-3} was installed perpendicular to the foundation surface, which can obtain the measured value at depth of 0 m, 2 m, 5 m and 10 m, respectively. Immediately after the excavation was finished, the maximum unloading displacement measured was 12.5 mm on 29 Dec 2014. When unloading displacement gradually became stable, the maximum displacement reached 16.8 mm (Fig. 15a). For the numerical result, the increment of unloading displacement at

EL 655 m is 12.2 mm (Fig. 15b). Unloading displacement values of numerical and measured results are listed in Table 6. In fact, owing to not considering the short time effect and the hypothesis of continuum and small strain, the numerical displacement of jointed rockmass could be slightly less than the field monitoring value. It is indicated that the unloading displacement at the foundation surface is mainly affected by the weak structural plane. Owing to sliding of the shear belt, the deformation of foundation rockmass at the hanging wall of the shear belt tends to vary at a high level.

The maximum increment of shear displacement of L_{S3319} and $L_{S3319-1}$ is 2.5 mm and 5.5 mm, respectively (Fig. 16). For the numerical result, the increment of shear displacement of

Table 4 Physical-mechanical parameters of rockmasses, fault and shear belts

Rock type	Density (kg/m^3)	Deformation modulus (GPa)	Poisson's ratio	Shear strength	
				Cohesion c (MPa)	Friction coefficient f
II	2800	18	0.23	1.4	1.3
III$_1$	2750	10	0.25	1.1	1.1
III$_2$	2600	8	0.27	0.75	0.9
IV	2500	3	0.3	0.5	0.7
F$_{17}$	2400	2	0.3	0.15	0.5
C$_3$	2400	0.71	0.3	0.10	0.39
C$_{3-1}$	2400	0.10	0.33	0.04	0.37
LS$_{331}$	2400	2.00	0.3	0.06	0.52
LS$_{3318}$	2400	0.30	0.33	0.1	0.42
LS$_{3319}$	2400	0.25	0.33	0.10	0.42
LS$_{3319-1}$	2400	0.25	0.33	0.09	0.4
LS$_{337}$	2400	0.2	0.33	0.05	0.37
LS$_{342}$	2400	0.3	0.33	0.1	0.5

L$_{S3319}$ and L$_{S3319-1}$ is 3 mm and 6.4 mm at the same position of monitoring points (Fig. 17a), respectively. During the excavation of EL 628~620 m and protective layer of EL 660~630 m, the shear displacement of L$_{S3319}$ and L$_{S3319-1}$ continued to increase, which is similar to the monitoring results (Fig. 17b). After the excavation of EL 660~620 m, pre-stressed anchorage cables are installed at foundation surface, and the shear displacement of L$_{S3319}$ and L$_{S3319-1}$ is stable during the excavation of EL 620~540 m (Fig. 17c, d). Thus, the shear belt mainly controls the stability of the dam foundation, and the pre-stressed anchorage cables are effective for preventing the sliding of shear belts.

Unloading relaxation analysis

The relaxation of joints is firstly evaluated by inverse analysis during the excavation from EL 645 m to EL 628. According to the monitoring results, the average relaxation depth at area B1 and C1 of experimental zone was 3.0 and 3.4 m, respectively. For numerical result, at experimental zone, the shear and tension failures occur in both joint sets with average relaxation depth of 3~3.5 m (Fig. 18a), which is close to the monitoring value.

During the excavation of EL 628 m to EL 620 m, the relaxation depth at hanging wall of L$_{S3319-1}$ deteriorates owing to the sliding of L$_{S3319-1}$ (Fig. 18a). When the protective layer of EL 660~620 m is excavated, a small part of relaxation zones remain at experimental zone and edge of shear belt L$_{S3319-1}$ (Fig. 18b). During the excavation of EL 620 m to EL 540 m, the maximum relaxation depth at foundation is 2 m near the steep slope at EL 585~575 m (Fig. 18c). After the protective layer is excavated, the relaxation zone is small (Fig. 18d). However, it should be noted that the blasting effect is not considered

Table 5 Deformation and strength parameters of rock and joint sets (Jin et al. 2015)

Rock type	Property	Value	Joint type	Property	Value
Rock mass	Deformation modulus (GPa)	20	Joint set 1	Spacing S_1 (m)	0.2
	Possion ratio	0.2		Cohesion c_1 (MPa)	0.75
	Cohesion c (MPa)	1.42		Friction coefficient f_1	0.70
	Friction coefficient f	0.75		Normal stiffness (GPa/m)	74
				Shear stiffness (GPa/m)	30
			Joint set 2	Spacing S_2 (m)	1.0
				Cohesion c_2 (MPa)	0.75
				Friction coefficient f_2	0.57
				Normal stiffness (GPa/m)	30
				Shear stiffness (GPa/m)	20

Fig. 14 Layout of deformation monitoring devices at the left foundation
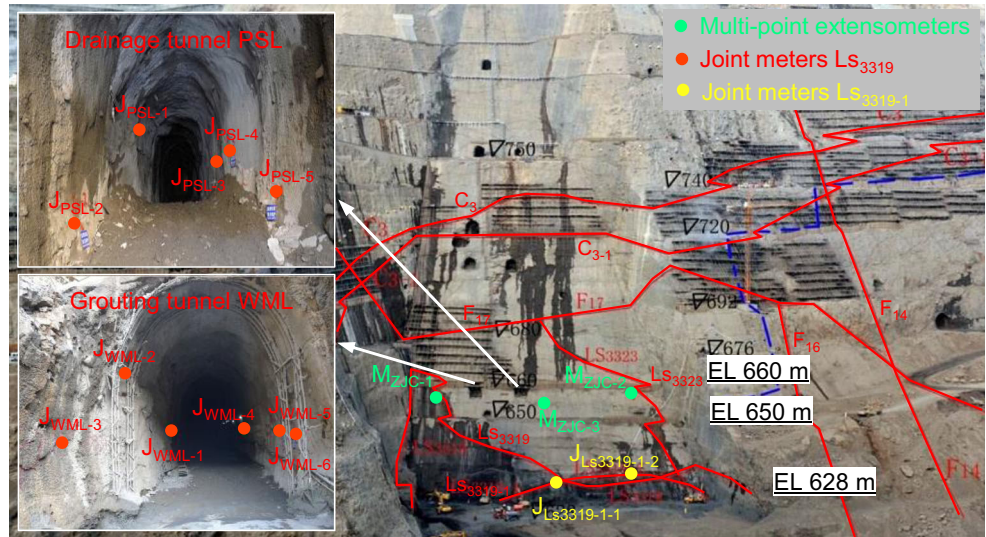
in the numerical simulation. Thus, the calculated yield zones could differ somewhat from the actual relaxation depth during foundation excavation.

In terms of the relaxation mode, the plastic zone in Fig. 18 shows that the relaxation of columnar joints mainly occurred at shallow foundation, particularly at

Fig. 15 Variation of deformation of category-I CJB: (a) variation of displacement with time monitored by multi-point extensometers; (b) magnitude and vector of displacement increment during excavation of EL 645~628 m (unit, m)
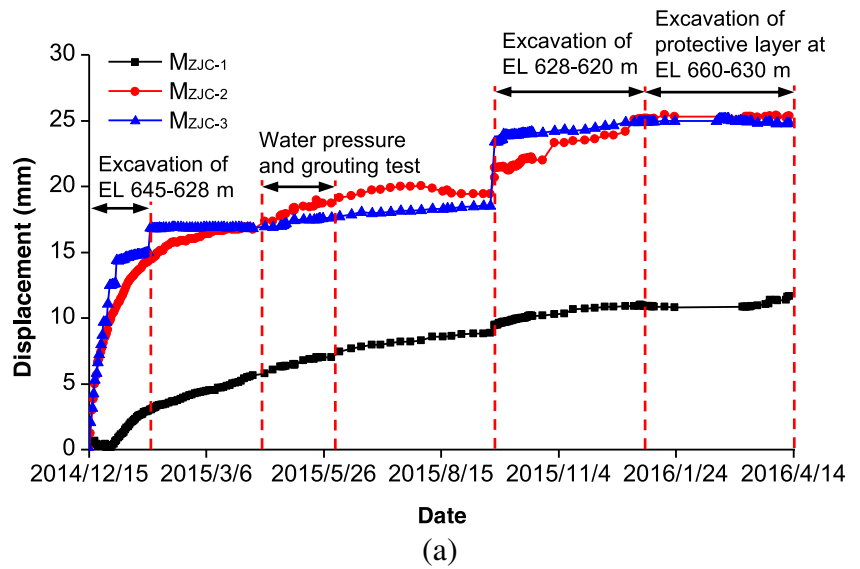

(a)

(b)
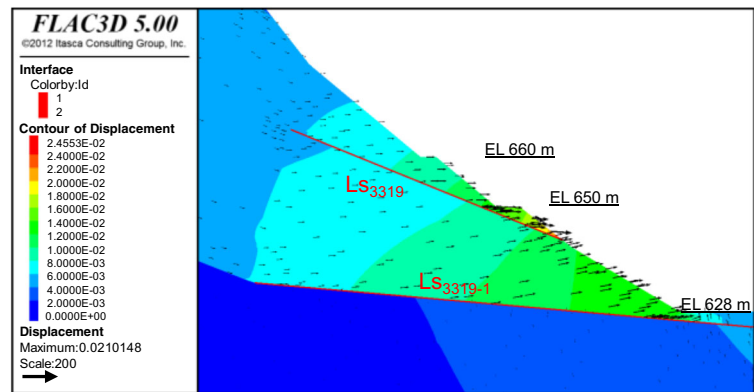
Table 6 Comparison of unloading displacement values between numerical and measured results

| Distance of measured point away from the foundation surface (m)	Numerical value (mm)	Measured value immediately after excavation completed (mm)	Measured value when unloading deformation becomes stable (mm)
0	12.2	12.5	16.8
2	11.8	12.2	16.3
5	9.3	10	13.6
10	9.5	10.5	14.0

the outcropping location of shear belts, which is consistent with the field relaxation condition. The relaxation mode is different under or out of the influence of shear belts. For the shallow relaxation of columnar joints, the surface layer of the rockmass rebounds towards the free face with gentle joints tensile and shear failure. For combined rebound deformation of columnar joints and shear belts, under the influence of sliding of shear belts, shear failure occurred in gentle joints when located at the hanging wall of shear belt and tensile failure occurred in steep joints. Particularly, below EL 650 m of foundation, tensile failure mainly occurred in steep joints at the hanging wall of steep shear belt Ls_{3319}, while tensile and shear failure occurred in gentle joints. Shear failure mainly occurred in gentle joints at the gentle shear belt Ls_{3319-1}.

Fig. 16 Variation of shear displacement recorded by joint meters: (a) Ls_{3319} in the grouting tunnel; (b) Ls_{3319} in the drainage tunnel and Ls_{3319-1} at the foundation surface
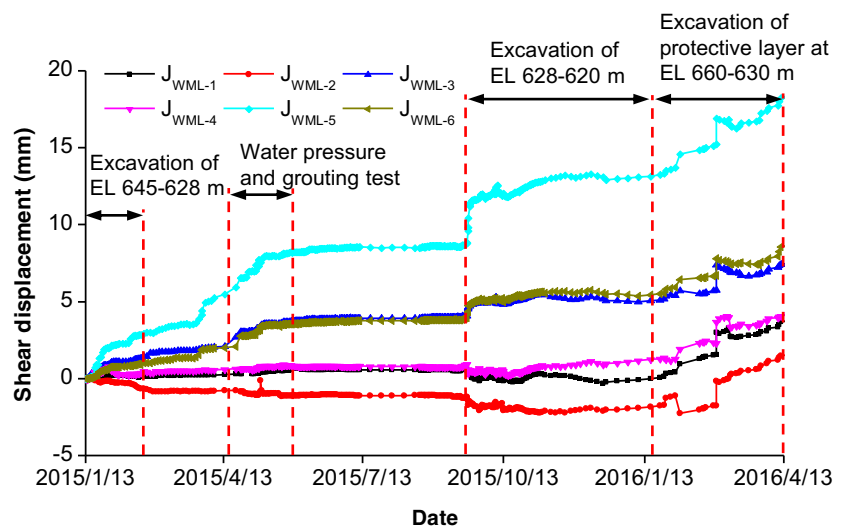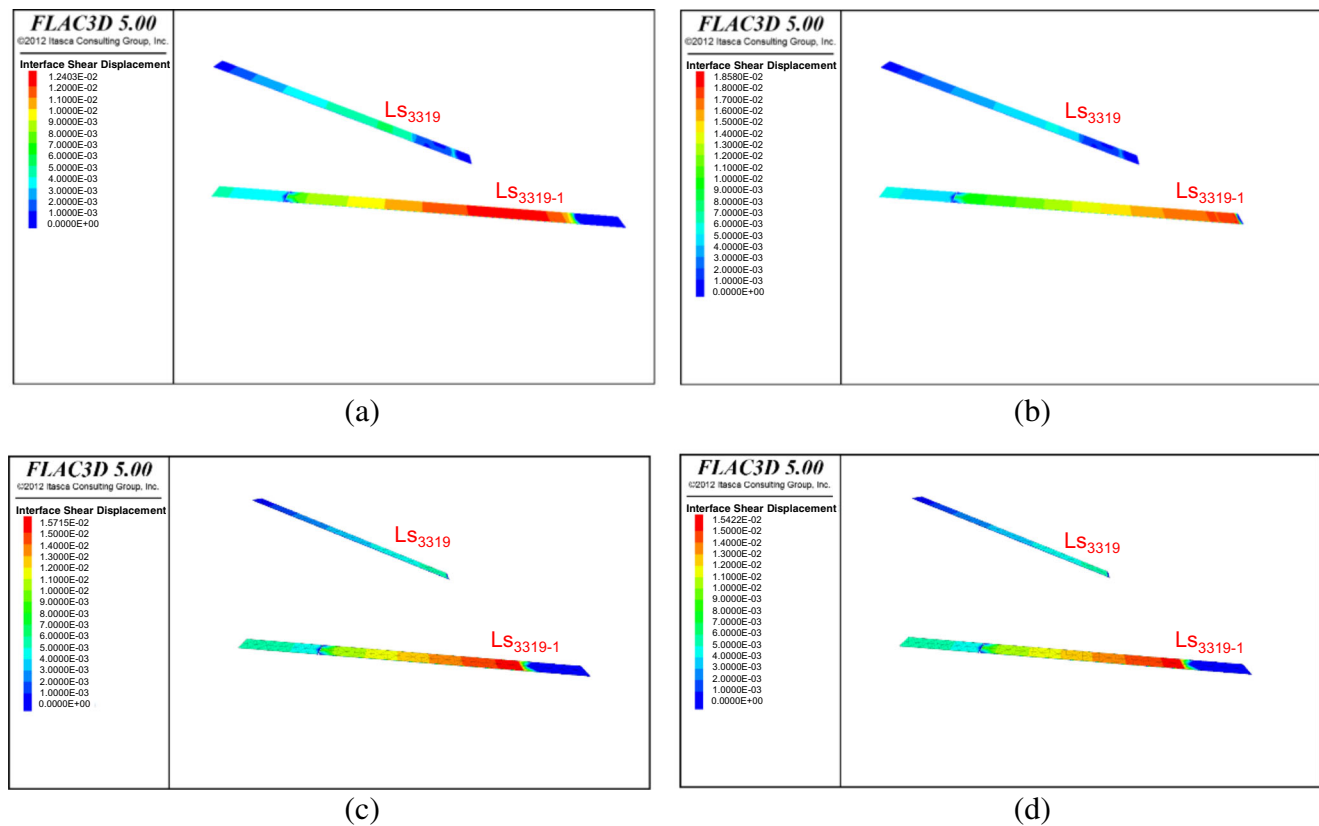

(a)
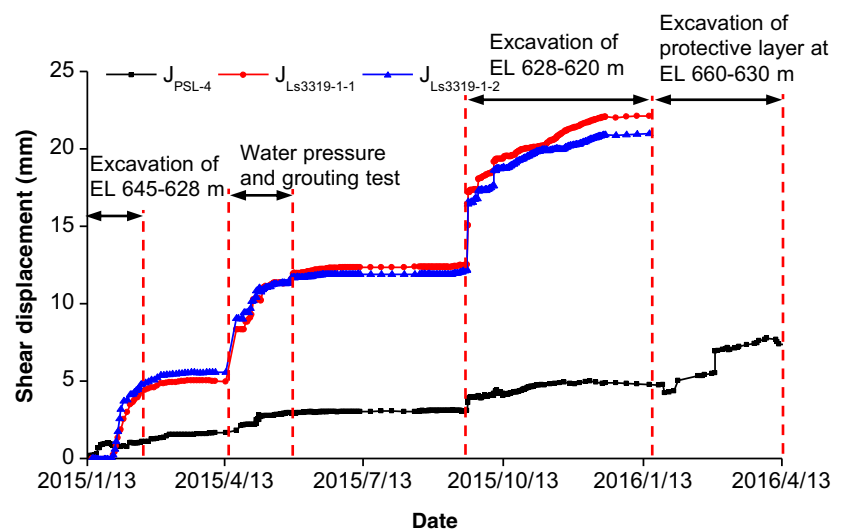
(b)

Fig. 17 Variation of shear displacement of shear belts Ls_{3319} and Ls_{3319-1} (Unit, m): (a) excavated to EL 628 m with protective layer; (b) excavated to EL 620 m with protective layer; (c) excavated to EL 620 m without protective layer; (d) excavated to EL 540 m with pre-stressed anchorage cables

Discussion on unloading relaxation mechanism

The excavation rockmass joints relaxation mechanism could be classified into three types: (1) rebound loose and shear slide of original joints; (2) cracking propagation of original joints; (3) new cracks emerged in intact rock. Through the field survey at the Baihetan dam foundation, the unloading joints at shallow foundation mainly belong to rebound loose and relaxation of original joints. Part of the new cracks were only found at superficial rockmass due to blast damage.

On the basis of the monitoring and numerical analysis, excavation unloading and blasting damage led to varying degrees of relaxation in the foundation rockmasses. In addition, the relaxation of category-I CJB could also be affected by joint condition, weak structural planes and complicated excavation outline. Shallow relaxation of columnar joints and combined rebound deformation of columnar joints and shear belts are two key unloading features. Thus, the unloading relaxation behaviours at the foundation surface are mainly related to the joint conditions in CJB as well as the weakening effect from the structural planes. Hao et al. (2016) summarized the

three main types of unloading failure mechanisms of CJB during excavation of diversion tunnels, i.e. failure caused by rockmass structures, high geo-stresses and a combination of geo-stresses and rockmass structures. For excavation of a dam foundation, the typical cracking behaviours are mainly controlled by rockmass structures (Hao et al. 2016).

In addition, the two types of unloading behaviours could be analysed from the point of geo-stress evolution. For shallow relaxation of columnar joints, during the excavation unloading, the maximum principal stresses gradually rotate towards free surface and decline to tensile stress zone at a certain depth, while minimum principal stresses maintain parallel with the dam interface. Thus, the surface layer of rockmass rebounds to the free face, mainly causing opening and sliding of shallow gentle joints. For combined rebound deformation of columnar joints and shear belts, the shear belts at foundation are the main windows to release geo-stress under excavation, which leads to shear slide. Many columnar joints and fissures are developed at the edge of shear belts. Thus, under the sliding influence of shear belts, the gentle joints at hanging wall of shear belts tend to occur with shear failure and steep joints open with tensile failure.
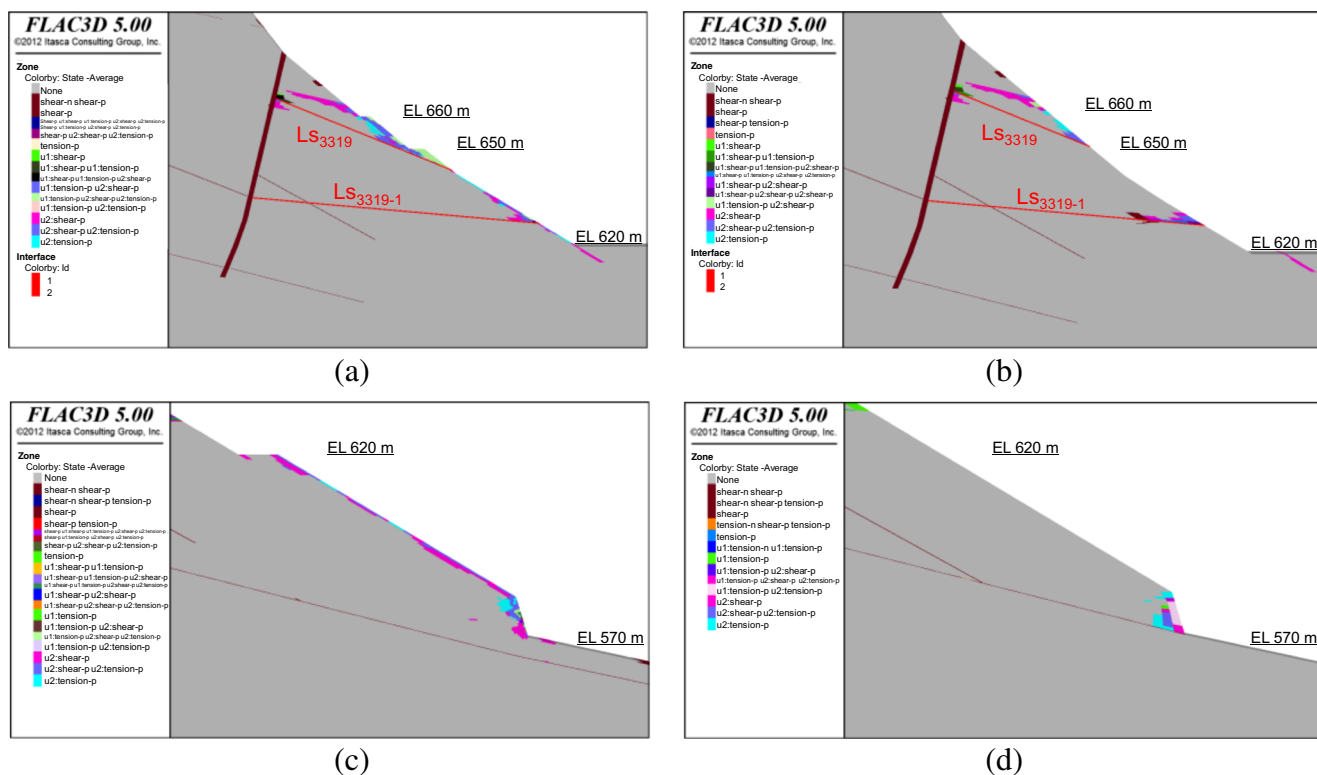
Fig. 18 Relaxation zones of category-I CJB at left foundation: (a) excavated to EL 620 m with protective layer; (b) excavated to EL 620 m without protective layer; (c) excavated to EL 545 m with protective layer; (d) excavated to EL 540 m without protective layer

Conclusions

In this study, the shallow unloading deformation characteristics and relaxation mechanism of CJB are analysed on the basis of field monitoring and numerical simulation for the Baihetan super-high arch dam. The main conclusions are:

(1) Unloading cracking features of CJB are revealed during excavation of the dam foundation, such as shallow relaxation of columnar joints and combined rebound deformation of columnar joints and shear belts. The typical cracking modes during foundation excavation are mainly controlled by rockmass structures.

(2) An equivalent continuum constitutive model was proposed for describing anisotropic deformation and failure behaviours, which can implicitly incorporate the discontinuities into constitutive equations. The numerical and monitoring results indicated that the proposed model can be applied to effectively simulate the unloading relaxation processes of dam foundation excavation.

(3) The monitoring and numerical simulation results indicate that the maximum relaxation depth of category-I CJB at the left foundation is 3~4 m, and the disturbance degree at the superficial rock layer of 1 m depth is relatively large. The relaxation degree is obviously exaggerated owing to the sliding of shear belts.

(4) The unloading relaxation mode at shallow foundation mainly belongs to rebound deformation and relaxation of original joints. The relaxation mechanism further reveals that the steep joints mainly fail with tensile cracking, and the gentle joint fails both with tensile and shear cracking.

References

Agharazi A, Martin CD, Tannant DD (2012) A three-dimensional equivalent continuum constitutive model for jointed rock masses containing up to three random joint sets. Geomech Geoeng 7:227–238

Chen SH, Wang GJ, Zhou H, Wang WM, Zou LC (2012) Evaluation of excavation-induced relaxation and its application to an arch dam foundation. Int J Numer Anal Met 36:166–181

Fan QX, Zhou SW, Yang N (2015) Optimization design of foundation excavation for Xiluodu super-high arch dam in China. J Rock Mech Geotech Eng 7:120–135

Fan QX, Feng XT, Weng WL, Fan YL, Jiang Q (2017) Unloading performances and stabilizing practices for columnar jointed basalt: a

case study of Baihetan hydropower station. J Rock Mech Geotech Eng 9:1041–1053

Fan QX, Wang ZL, Xu JR, Zhou MX, Jiang Q, Li G (2018) Study on deformation and control measures of columnar jointed basalt for Baihetan super-high arch dam foundation. Rock Mech rock Eng. 51:2569–2595

Gardner GHF, Gardner LW, Gregory AR (1974) formation velocity and density-the diagnostic basics for stratigraphic traps. Geophysics 39: 770–780

Goehring L, Morris SW, Lin Z (2006) An experimental investigation of the scaling of columnar joints. Phys Rev E 74:1–13

Hao XJ, Feng XT, Yang CX, Jiang Q, Li SJ (2016) Analysis of EDZ development of columnar jointed rock mass in the Baihetan diversion tunnel. Rock Mech Rock Eng 49:1289–1312

Hatzor YH, Feng XT, Li SJ, Yagoda-Biran G, Jiang Q, Hu LX (2015) Tunnel reinforcement in columnar jointed basalts: the role of rock mass anisotropy. Tunn Undergr Sp Tech 46:1–11

Iwata N, Sasaki T, Yoshinaka R, Kurooka K (2012) Applicability of the multiple yield model for estimating the deformation of vertical rock walls during large-scale excavations. Int J Rock Mech Min Sci 52: 171–180

Jiang Q, Feng XT, Hatzor YH, Hao XJ, Li SJ (2014) Mechanical anisotropy of columnar jointed basalts: an example from the Baihetan hydropower station, China. Eng Geol 175:35–45

Jin CY, Yang CX, Fang D, Xu S (2015) Study on the failure mechanism of basalts with columnar joints in the unloading process on the basis of an experimental cavity. Rock Mech Rock Eng 48:1275–1288

Jin CY, Li SG, Liu JP (2018) Anisotropic mechanical behaviors of columnar jointed basalt under compression. B Eng Geol Environ 77(1):317–330

Lin P, Wang RK, Zhou YN, Zhou WY (2008) Study of shallow unloading mechanism and stability of foundation surface of super high arch dam. Rock Soil Mech 29:8–14 (in Chinese)

Lin P, Ma TH, Liang ZZ, Tang CA, Wang RK (2014) Failure and overall stability analysis on high arch dam based on DFPA code. Eng Fail Anal 45:164–184

Lin P, Zhou WY, Liu HY (2015) Experimental study on cracking, reinforcement and overall stability of the Xiaowan super high arch dam. Rock Mech Rock Eng 48(2):819–841

Lin P, Zhu XX, Li QB, Liu HY, Yu YJ (2016) Study on optimal grouting timing for controlling uplift deformation of a super high arch dam. Rock Mech Rock Eng 49(1):115–142

Lin P, Shi J, Zhou WY, Wang RK (2018) 3D geomechanical model tests on asymmetric reinforcement and overall stability relating to the Jinping I super-high arch dam. Int J Rock Mech Min Sci 102:28–41

Malmgren L, Saiang D, Töyrä J, Bodare A (2011) The excavation disturbed zone (EDZ) at Kiirunavaara mine, Sweden–by seismic measurements. J Appl Geophys 61:1–15

Shen XM, Niu XQ, Lu WB, Chen M, Yan P, Wang GH, Leng ZD (2017) Rock mass utilization for the foundation surfaces of high arch dams in medium or high geo-stress regions: a review. B Eng Geol Environ 76:795–813

Shen XM, Chen M, Lu WB, Li L (2016) Using P wave modulus to estimate the mechanical parameters of rock mass. B Eng Geol Environ 76:1461–1470

Shi AC, Tang MF, Zhou QJ (2008) Research of deformation characteristics of columnar jointed basalt at Baihetan hydropower station on Jinsha river. Chin J Rock Mech Eng 27:2079–2086 (in Chinese)

Shi AC, Tang MF, Shan ZG (2015) Engineering geology report for the excacation and treatment at the left abutment and riverbed foundation of Baihetan hypropower station. Power China Huadong engineering corporation limited, Hangzhou (in Chinese)

Shi J, Lin P, Zhou YD, Wei PC (2018) Wang RK(2018) reinforcement analysis of toe blocks and anchor cables at the Xiluodu super-high arch dam. Rock Mech Rock Eng 51(8):2533–2554

Singh B (1973) Continuum characterization of jointed rock masses: Part I—The constitutive equations. Int J Rock Mech Min Geomech Abstracts 10:311–335

Wang TT, Huang TH (2009) A constitutive model for the deformation of a rock mass containing sets of ubiquitous joints. Int J Rock Mech Min Sci 46:521–530

Wu FQ, Liu JY, Liu T, Zhuang HZ, Yan CG (2009) A method for assessment of excavation damaged zone (EDZ) of a rock mass and its application to a dam foundation case. Eng Geol 104:254–262

Xiao YX, Feng XT, Chen BR, Feng GL, Yao ZB, Hu LX (2017) Excavation-induced microseismicity in the columnar jointed basalt of an underground hydropower station. Int J Rock Mech Min Sci 97: 99–109

Xu WY, Zheng WT, Shi AC (2011) Classification and quality assessment of irregular columnar jointed basaltic rock mass for hydraulic engineering. J Hydraul Eng 42:262–270 (in Chinese)

Zhang YZ, Lu WB, Chen M, Yan P, Hu YG (2013) Dam foundation excavation techniques in China: a review. J Rock Mech Geotech Eng 5:460–467